Intrinsic Constraints of Neural Origin: Assessment and Application to Rehabilitation Robotics

Domenico Campolo, *Member, IEEE*, Dino Accoto, *Member, IEEE*, Domenico Formica, and Eugenio Guglielmelli, *Member, IEEE*

***Abstract*—Ideally, robots used for motor rehabilitation, in particular, during assessment, should minimally perturb the voluntary movements of a subject. In this paper, we show how a state-of-the-art back-drivable robot, i.e., a robot that can be moved by the user with a low perceived mechanical impedance, when used for assessment can still perturb the voluntary movements of a subject. In particular, we show that, despite its low mechanical impedance, a robot may still not comply with the intrinsic kinematic constraints, which are of neural origin and are adopted by the human brain to solve redundancy in motor tasks. Specifically, the redundant task under consideration is the 2-D pointing task, which is performed by a subject with the sole use of the wrist [3 degree of freedom (DOF) kinematics]. Wrist orientations during pointing tasks are assessed in two different scenarios. In the first experiment, a lightweight handheld device is used, which introduces no loading effect. In the second experiment, similar pointing tasks are performed with the subject interacting with a state-of-the-art robot for wrist rehabilitation. In the first case, intrinsic kinematic constraints arise as 2-D surfaces embedded in the 3-D space of wrist configuration. Such surfaces are typically subject-dependent and reveal personal motor strategies. In the second case, a strong influence of the robot is remarked. In particular, 2-D surfaces still arise but are similar for all subjects and are referable to a mechanical origin (excessive loading by the robot). The assessment approach described in this paper, including both the experimental apparatus and data-analysis method, can be used as a test for the degree of back-drivability of mechanisms and robots in relation to constraints of neural origin, thus allowing the design of robots that can actually cope with such constraints. The clinical potential impact is also discussed.**

***Index Terms*—Back-drivability, Donders' law, human motor control, intrinsic kinematic constraints, wrist robots.**

I. Introduction

RECENT years have witnessed an increase of the interest in robot-mediated motor therapy. In the last two decades, various robots have been proposed that specifically target different areas of neurorehabilitation, ranging from upper to lower limbs, from proximal to distal joints [1]–[11]. Rehabilitation robots can be used for both therapy and assessment. In the case of therapy, correcting forces/movements can be delivered/imparted by the robot to the subject to help the completion of motor tasks. Therapy and assessment sessions can be interlaced, and assessment sessions may determine the amount of future therapy to be imparted; therefore, assessment may have an indirect impact on therapy.

The design of most of the robots for neurorehabilitation hinges upon the widely accepted principle that the patient must have an active role in the execution of the motor task. This basic principle has a profound impact on the technological choices regarding the mechanical structure and the control system of the robot [12]. Indeed, the voluntary movements of the users should be minimally perturbed by the physical interaction with the robot, especially during assessment. During therapy, the robot should assist the patients only when they are not able to complete the task autonomously. Also, the level of assistance should be tuned according to the patients' residual abilities [13]. The kinematics of the robot in terms of both the workspace geometry and the ranges of motions of each link should, in the first place, match the constraints imposed by the biomechanics of the human body. Moreover, special attention is devoted to achieving a high degree of back-drivability, i.e., the ability of the robot being moved by the user with a low perceived mechanical impedance [14] in order not to hinder any voluntary motions involved in the specific task. One of the most distinctive features of neurorehabilitation robots refers to the ability of such systems to match the kinematic constraints of the human body while offering a low perceived mechanical impedance during user-driven motions. This is especially true during assessment, when no corrective forces/movements are delivered/imparted by the robot, and the subject is in charge of moving his/her limb as well as the mechanisms of the robots while performing the motor task. The major contribution of this paper is to show that besides "hard" (biomechanical) constraints, the design of robots physically interacting with humans should also consider another class of "soft" constraints: those with a *neural origin*. In particular, this paper describes a method to assess such constraints during redundant motor tasks performed with and without the use of the robot. The influence of the robot is revealed by comparing the different outcomes.

Before proceeding, some scientific background on neural constraints and how these relate to the degrees of freedom (DOFs) problem in redundant motor tasks shall be provided. To the authors' knowledge, the clinical implications of such issues for rehabilitation robotics have never been addressed in the literature.

Manuscript received February 20, 2009; revised March 19, 2009. First published April 24, 2009; current version published June 5, 2009. This paper was recommended for publication by Associate Editor M. Johnson and Editor K. Lynch upon evaluation of the reviewers' comments. This work was supported in part by the European Commission within the Thought in Action (TACT) Project (FP6-NEST/ADVENTURE Program under Contract 015636) and in part by the NEUROBOTICS Project, which is the fusion of Neuroscience and Robotics under FP6-IST-001917).

The authors are with the Biomedical Robotics and Biomicrosystems Laboratory, Center for Integrated Research, Università Campus Bio-Medico, 00128 Rome, Italy (e-mail: campolo@sssup.it; d.accoto@unicampus.it; d.formica@unicampus.it; e.guglielmelli@unicampus.it).

Color versions of one or more of the figures in this paper are available online at http://ieeexplore.ieee.org.

Digital Object Identifier 10.1109/TRO.2009.2019781

A. Intrinsic Constraints of Neural Origin: Redundancy Problem

The human motor system often needs to cope with kinematic redundancies: we generally have many more DOFs than necessary to fulfill the requirements of the task. The coordination of kinematically redundant systems was first formulated by Bernstein as the *redundancy problem* [15].

Two main approaches to the DOFs problem can be recognized in literature: global and local approaches.

Global approaches start from an *a priori* hypothesis and propose minimum principles in which a global cost function is assumed to be minimized by the central nervous system, thus leading to optimal behavior, which also solves the redundancy problem. Main theories are minimum effort, minimum jerk [16], minimum torque change [17], minimum variance [18], and uncontrolled manifold [19], [20].

Local approaches seek invariants at the level of measurable movement variables, and this gives rise to empirical laws such as Donders'/Listing's law [21], Fitt's law, isochrony [22], linearly related joint velocities [23], straight path and bell-shaped velocity profiles [24], and "two-third power law" [25]. While the former are motor control theories that attempt to explain phenomena, the latter are empirical and descriptive and are therefore more operative.

When it comes to solving kinematic redundancies, it is known that the brain imposes constraints that 1) reduce the DOF to the necessary ones and 2) implement strategies for motor efficiency. Such constraints of neural origin are also referred to as *intrinsic* [28], or "soft." Historically, the first examples of such intrinsic constraints were found in the oculomotor domain. In a good approximation, the eye can be considered as a center-fixed sphere rotated by the action of six (i.e., three agonist–antagonist couples) extra ocular muscles (EOMs). EOMs provide 3-DOF kinematics, thus allowing full mobility in the space of rigid body rotations with the only limitations given in terms of range of motion. When looking at some point in space, the gaze direction is fully determined but not the amount of ocular torsion about the line of sight. In other words, for a given line of sight, uncountably many eye configurations (torsions) exist that correspond to the same gaze direction.

In 1847, Donders experimentally found that for a given *steady* gaze direction, there is only one eye configuration (*Donders' law*) [26]. In other words, physiological eye configurations are described by a 2-D surface embedded into the 3-D space of eye configurations: a solution to redundancy. Two decades later, Listing and Helmholtz went one step further, determining that such a 2-D surface is actually a *plane*; the eye assumes only those positions that can be reached from primary position by a single rotation about an axis in the *Listing's plane*, which lies orthogonal to the gaze direction in primary position (*Listing's law*) [26]. Listing's law is, therefore, a particular form of a more general Donders' law; the former prescribes a plane, whereas the latter prescribes a generic surface. In this paper, we shall refer, in general, to Donders' laws.

It had been debated for quite some time whether Donders' law was due to a biomechanical or a neural mechanism. It is now known that such a law holds during fixation, saccades, smooth pursuit, and vergence but not during sleep and vestibulo-ocular reflex, which suggest that it is actively implemented by a neural mechanism [27].

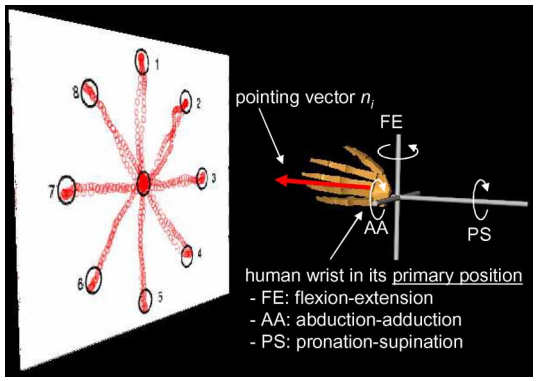

Fig. 1. Typical "video game" for guiding a subject through pointing tasks.

In the last two decades, Donders' law has been found to apply well to the head as well as to the limb movements. See [21] for a comprehensive collection of such works, as well as more recent papers such as [28] and references therein. It is interesting to note how these results further support the neural origin for Donders' law, since, differently from the oculomotor system, the human subject has voluntary control over the DOF involved in both head and limb movements, which may, therefore, span the full dimensionality of the configuration space.

B. Human Wrist: Redundancy During Pointing Tasks

In order to investigate the effects of a physical interaction between robots and humans when "soft" constraints (arising in redundant motor tasks) are involved, we identified the human wrist as an optimal candidate among all possible motor districts mainly for two sets of reasons. On one hand, the human wrist has only 3 DOF, yet redundancy issues still arise in natural tasks such as pointing (the upper limb could be another possible candidate but it is kinematically much more complex). On the other hand, restoring lost functionality of the upper limb is of great interest for neurorehabilitation, and recently, specific robots for wrist rehabilitation have been proposed. In particular, the InMotion3 wrist robot (the extension module of the MIT-MANUS robot from Interactive Motion, Inc.) [3], [29] is a rotational 3-DOF robot, specifically designed to kinematically conform to the natural rotations of human wrist as well as to generate programmable torque fields used during rehabilitation.

As for the motor tasks, typical rehabilitation sessions for the InMotion3 wrist robot make use of "video games" as the one in Fig. 1; the patient grasps a handle and, with his/her torso, upper and lower arm fastened to an arm support, performs 2-D pointing tasks toward targets displayed on a screen (from/to the central target to/from the peripheral ones) with the use of the 3-DOF wrist kinematics. Redundancy is a common feature of many rehabilitation tasks.

The InMotion3 wrist robot, the state of the art for wrist neurorehabilitation was carefully designed to comply with the

biomechanical ("hard") constraints of the human wrist and to provide a high degree of back-drivability [29] but *are these features sufficient to also comply with "soft" constraints, at least during assessment sessions?* Answering this question is important to ensure that the robot does not perturb the subject's intrinsic motor strategies, which are often deployed by the brain to optimize motor efficiency.

In what follows, we first describe an operative method to assess a subject's soft constraints, in particular, for the human wrist during pointing tasks, and then, we show how physical interaction with a robot might still allow the subject to successfully complete the motor task but by means of different motor strategies.

Before proceeding, basic mathematical tools for describing the geometry of rotations will be briefly reviewed (see [30]–[32]).

II. Rotations, Gimbals, and Wrist Kinematics

Rotations in the Euclidean space $\mathbb{R}^3$ can be described by the *group* of 3×3 orthonormal matrices

$$SO(3) = \{R \in \mathbb{R}^{3\times 3} : R^T R = I, \det R = +1\}$$

where I is the 3×3 identity matrix. Any orientation $R \in SO(3)$ is equivalent to a rotation about a fixed axis $\mathbf{v} \in \mathbb{R}^3$ through an angle $\theta \in [0, 2\pi)$ [33, Euler's theorem].

A rotation matrix R can be seen as a mapping $R : \mathbb{R}^3 \to \mathbb{R}^3$ and represented in $\mathbb{R}^3$ (i.e., the same space it acts upon) via a *rotation vector* $\mathbf{r} = [r_x, r_y, r_z]^T \in \mathbb{R}^3$, which defines the axis (parallel to $\mathbf{r}$ itself) and the amount of rotation [$\|\mathbf{r}\| = \tan(\theta/2)$]. As shown in [31], for a generic rotation R, the corresponding rotation vector is

$$\mathbf{r} = \frac{1}{1 + R_{1,1} + R_{2,2} + R_{3,3}} \begin{bmatrix} R_{3,2} - R_{2,3} \\ R_{1,3} - R_{3,1} \\ R_{2,1} - R_{1,2} \end{bmatrix} \tag{1}$$

where $R_{i,j}$ represents the (i, j) element of the matrix R.

Rotations about principal axes (x-, y-, and z-axis) can be written as

$$R_x(\theta) = \begin{bmatrix} 1 & 0 & 0 \\ 0 & \cos\theta & -\sin\theta \\ 0 & \sin\theta & \cos\theta \end{bmatrix} \tag{2}$$

$$R_y(\theta) = \begin{bmatrix} \cos\theta & 0 & \sin\theta \\ 0 & 1 & 0 \\ -\sin\theta & 0 & \cos\theta \end{bmatrix} \tag{3}$$

$$R_z(\theta) = \begin{bmatrix} \cos\theta & -\sin\theta & 0 \\ \sin\theta & \cos\theta & 0 \\ 0 & 0 & 1 \end{bmatrix}. \tag{4}$$

For solving a pointing task, only 2 DOF would suffice. Examples of mechanical systems with 2 DOF are the Fick's and Helmholtz's gimbals in Fig. 2, where the order of rotation (of an angle θ_v about the vertical axis and θ_h about the horizontal axis) is mechanically imposed by the structure of the system

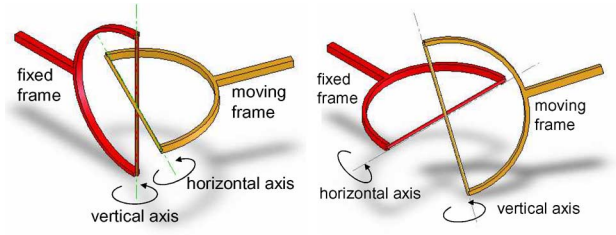

Fick-gimbal Helmholtz-gimbal

Fig. 2. Fick and Helmholtz gimbals.

$$R_{\text{Fick}} = R_z(\theta_v) R_y(\theta_h) \tag{5}$$

$$R_{\text{Helm}} = R_y(\theta_h) R_z(\theta_v). \tag{6}$$

One of the main characteristics of $SO(3)$ is the *noncommutativity* property of the group and, in general, $R_{\text{Fick}} \neq R_{\text{Helm}}$, i.e., in a sequence of rotations, the order matters. In general, a couple of angles (θ_v, θ_h) that leads to a given pointing direction would be different according to whether a Fick gimbal or a Helmholtz gimbal is used.

Via straightforward calculations, i.e., by applying the definition (1) to both (5) and (6), it can be verified that for Fick and Helmholtz gimbals, the following holds:

$$\begin{aligned} r_x &= -r_y\, r_z \qquad \text{(Fick)} \\ r_x &= +r_y\, r_z \qquad \text{(Helmholtz)} \end{aligned} \tag{7}$$

where r_x, r_y, and r_z represent the components of $\mathbf{r}$, i.e., the rotation vector.

Equations (7) represent, respectively, for the Fick and the Helmholtz gimbals, constraints for the achievable orientations. In particular, in the 3-D $SO(3)$ space, only those orientations can be achieved whose rotation vectors lie on the surfaces defined by the quadratic forms in (7). Of course, this was expected since the mechanical structures of the Fick and Helmholtz gimbals only allow 2 DOF, and this translates into a 2-D manifold embedded in $SO(3)$.

On the other hand, the existence of a 2-D manifold implementing not a biomechanical but a neural constraint (Donders' law) for a 3-DOF system such as the human eye is remarkable, since it denotes a *simplifying* strategy of the motor system.

III. Assessing Intrinsic Constraints for the Human Wrist

The existence of a Donders" law for the human wrist remains a conjecture. Nevertheless, here we will employ it as a means to test the back-drivability of a robot with respect to "soft" constraints and will be thoroughly described in this section.

A. Materials and Methods

Ten healthy subjects, aged between 25 and 35 years, were asked to complete a series of pointing tasks. As shown in Fig. 3, each subject was strapped to a chair, and one arm was supported by appropriate belts to minimize torso and shoulder and elbow

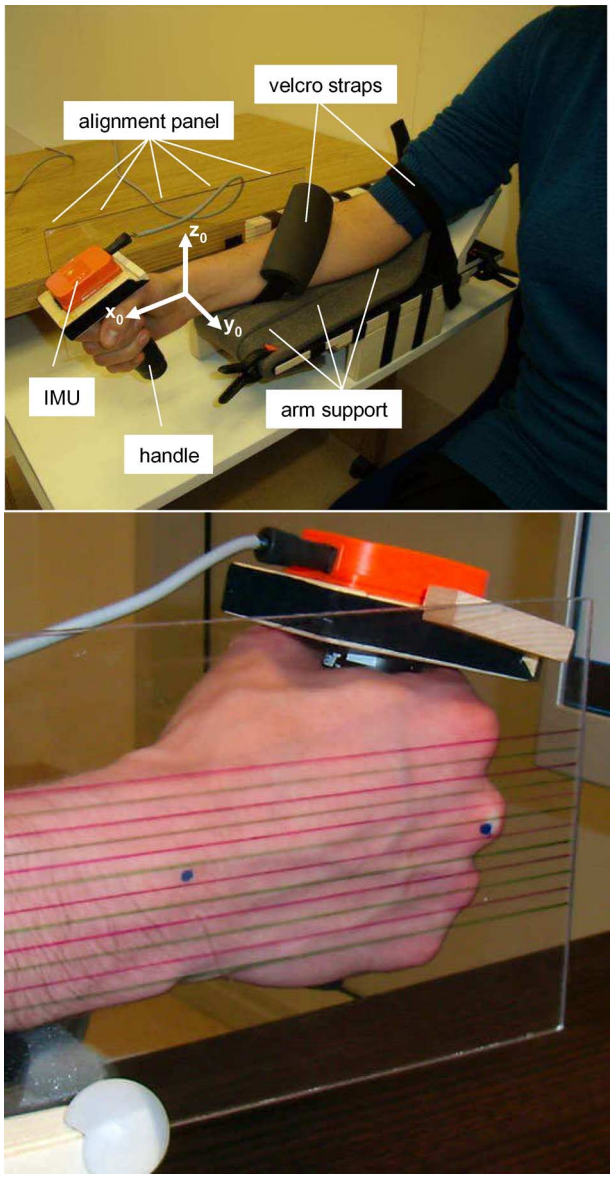

Fig. 3. (Top) Experimental apparatus for trials with the handheld device. For each subject, the alignment panel, which is made of transparent plexis glass, is only used for the initial setup of the primary position and removed during the execution of the trial. (Bottom) Detail of the sliding panel with the parallel lines used to easily align the abduction–adduction DOF to its anatomical neutral position.

movements so that only wrist rotations were left unconstrained. The orientation $R \in SO(3)$ of the wrist was measured by means of an Inertial Magnetic Unit (IMU, MTx-28A33G25 device from XSens, Inc.; static orientation accuracy: $<1^\circ$; bandwidth: 40 Hz) mounted on top of a hollow cylindrical handle (height: 150 mm, outer diameter: 50 mm, inner diameter: 35 mm, mass: 120 g) which each subject was asked to grasp firmly during the experiment. In what follows, such an apparatus is referred to as a *handheld* device.

The IMU, which was connected to a PC, was configured to continuously acquire the sequence of orientation matrices R_i (relative to the ith sample) at a rate of 100 samples/s.

Before starting the trial, a "zero" position for the wrist, also referred to as the *primary position*, was defined by means of a vertical sliding panel (see Fig. 3), which was then removed for the execution of the trial for each subject. In particular, the panel allowed aligning the wrist to its neutral position, as defined by the International Standard of Biomechanics (ISB) [34].

With the wrist in its primary position, a fixed reference frame $\{x_0, y_0, z_0\}$, also shown in Fig. 3, was defined as follows:

1) z_0-axis: along the vertical direction (upwards);
2) x_0-axis: horizontal, aligned with the forearm (forward);
3) y_0-axis: horizontal and perpendicular to the forearm (leftward).

A second reference frame $\{x, y, z\}$ attached to the wrist (moving frame) was defined to coincide with the fixed reference frame when the wrist is in the primary position.

In order to reduce computational complexity, the primary position was also selected as the "home" position for the IMU, meaning that the coordinates of the x-, y-, and z-axis with respect to the fixed frame $\{x_0, y_0, z_0\}$ could be determined, respectively, as the first, the second, and the third columns of the matrix R_i. To this aim, a software *reset procedure* for the IMU device must be performed while the wrist is held still in the primary position.

For a generic orientation R_i, the *pointing vector* (always parallel with the moving x-axis after the reset procedure) can then be determined as the first column of R_i

$$\mathbf{n}_i = R_i \, [1 \;\; 0 \;\; 0]^T. \tag{8}$$

A computer screen was used to display the "video game" according to the protocol given shortly where (see Fig. 1) the position of a round cursor is determined, in real time, directly by the orientation of the subject's wrist. In particular, the screen was physically located on the vertical plane in front of the subject (the y_0–z_0 plane), and the position of the cursor was determined by the projection of the pointing vector $\mathbf{n}_i$ onto the y_0–z_0 plane. This would, in fact, reproduce the physical sense of pointing a laser beam at the screen, without involving geometric remapping between unrelated frames of reference.[1]

The position of the cursor is given by the second and the third components of the vector $\mathbf{n}_i$. A rotation of 0.5 rad of the wrist for flexion–extension and 0.25 rad in the abduction–adduction is required to move the cursor from the central position to any of the peripheral positions in Fig. 1.

The session starts with the subject in the primary position and, therefore, with the cursor projected onto the central position of the video game. The subject is then instructed to move the round cursor on the screen toward the peripheral positions randomly chosen among "1," "2," . . . , "8" (see in Fig. 1) and, then, back to the central position. One trial is completed when all the eight peripheral positions are reached.

After five initial learning trials to get acquainted with the experimental setup, each subject was then asked to repeat the trial five times. Only the latter trials would then be used for data analysis.

[1] As in the case of a computer, the mouse moved horizontally on the desk and produced vertical movements on the computer screen.

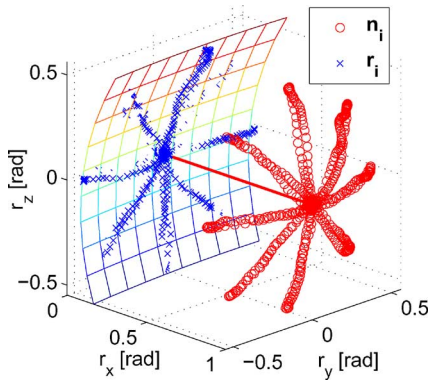

Fig. 4. Rotation vectors (crosses) are represented (in radians) in the 3-D space of the motor task together with the pointing vectors (circles). A 2-D quadratic surface (Donders' surface) fits the rotation vectors with a 0.029 rad (1.67°) deviation (thickness).

B. Experimental Results for the Handheld Device

The sequences of rotation matrices R_i acquired during the five trials were analyzed as follows.

Given the sequence R_i relative to each trial, the sequence of rotation vectors $\mathbf{r}_i$ and the sequence of pointing vectors $\mathbf{n}_i$ were derived via (1) and (8), respectively. As an example, both sequences of a single trial are plotted in Fig. 4. Here, it is worth recalling the *geometrical* interpretation of $\mathbf{r}_i$: at any time t_i, the orientation R_i of the wrist can be achieved from the primary position by a *single rotation* about the vector $\mathbf{r}_i$ of an angle $\theta_i = 2\arctan(\|\mathbf{r}_i\|)$. Such an interpretation allows representing rotations in the same 3-D space of the motor task. In Fig. 4, both the wrist pointing directions $\mathbf{n}_i$ (circles) and the rotation vectors[2] $\mathbf{r}_i$ (crosses) are represented. While the wrist pointing directions necessarily lie in a 2-D space,[3] the three components r_{xi}, r_{yi}, and r_{zi} of a rotation vector $\mathbf{r}_i$, in general, define points of a 3-D space. Remarkably, it can be observed that the rotation vectors tend to lie on a 2-D surface (Donders' law), which can be well approximated by a plane (Listing's plane) near the primary position.

Numerically, the sequence $\mathbf{r}_i = [r_{xi} \;\; r_{yi} \;\; r_{zi}]^T$ was fitted as in [26] to a generic quadratic surface

$$r_{xi} = C_1 + C_2 r_{yi} + C_3 r_{zi} + C_4 r_{yi}^2 + 2C_5 r_{yi} r_{zi} + C_6 r_{zi}^2 \tag{9}$$

where the coefficients $C_1, \ldots, C_6$ were determined via nonlinear least squares fitting methods.[4] The first three coefficients (C_1, C_2, and C_3) define a plane (Listing's plane), while the last three coefficients (C_4, C_5, and C_6) are related to the *curvature* of the fitted surface (see [35]). In particular, the coefficient C_5 denotes the amount of *twisting* of a quadratic surface.

Deviation from the best fitting surface, i.e., the *thickness* of a Donders' surface, is defined as the standard deviation of the sequence $\mathbf{r}_i$ from the surface defined by (9).

[2]In fact, vectors of length θ_i instead of $\|\mathbf{r}_i\|$ are represented so that the amount of rotation (in radians) can be visually derived, e.g., as in [28].

[3]Pointing vectors $\mathbf{n}_i$ are unit-length vectors, and therefore, their end tips lie on a sphere, as shown in Fig. 4.

[4]The function `nlinfit` in the MATLAB environment from MathWorks, Inc., was used.

For each subject, the values of the $C_1, \ldots, C_6$ coefficients (as well as of the thickness) averaged over the five trials are reported (in the form of mean value and standard deviation) in each row of Table I and used to define an averaged Donders' surface. Fig. 6(a) shows ten superimposed averaged surfaces, one for each subject. In Fig. 6(b), the averaged coefficients are represented in form of histogram with vertical bars representing the 95% confidence interval. Although numerically related to the standard deviation, the confidence interval allows direct testing for statistical significance. For example, if the confidence interval of a generic coefficient C_i does not include zero, then C_i can be considered statistically different from zero. This is the case, for example, for the C_4, C_5 and C_6 coefficients of several subjects, meaning that surfaces are, in fact, nonplanar and justify a nonlinear (higher order) fitting.

Remark: Thicknesses in the order of 0.02–0.03 rad, as in Table I, for angular excursions of 0.5 rad for flexion–extension and 0.25 rad for abduction–adduction are found to be in line with deviations for the oculomotor system [26] or for the upper limbs [28], and are explained as "biological noise" by Tweed and Vilis [26].

IV. Applying the Conjecture That Donders' Law is Valid for the Human Wrist When Connected to a Wrist Robot

In this section, the conjecture that Donders' law holds for the human wrist during pointing tasks is tested when the subject is connected to the InMotion3 wrist robot. Such a robot is equipped with motors that can generate programmable torque fields used to deliver forces or impart movements during therapy. In particular, during therapy, the robot can be programmed to represent variable impedances (by setting the control stiffness and damping parameters) to help the patient who is unable to complete a specific motor task. For the experiments described in this section, the motors are set to the so-called zero-impedance mode, i.e., the control stiffness and damping parameters are both set to zero value. In this modality, the only active role of the motors is to compensate gravity.

A. Materials and Methods

Ten healthy subjects (different from the previous experiment), aged between 25 and 35 years, were asked to complete a series of pointing tasks. Each of them was strapped to a chair and an arm support by appropriate belts to minimize torso and shoulder and elbow movements so that only wrist rotations were left unconstrained. The subject was then attached to the InMotion3 wrist robot. The wrist module consists of a mechanism that is able to conform to wrist rotations once the forearm of the subject is strapped onto the module and the subject grasps a handle, which is also part of the module. The starting position for the wrist was set as to coincide with the mechanical zero position of the robot, as defined in [3].

The sequence of mechanical joints that allow the mechanism to conform to the 3-DOF wrist rotations, as derived from [29], is represented in Fig. 5. In particular, the following angles

TABLE I
EACH ROW REPORTS THE VALUES AVERAGED OVER FIVE TRIALS FOR EACH SUBJECT RELATIVE TO THE TESTS WITH THE HANDHELD DEVICE

subjects	C_1 [rad]	C_2	C_2	C_4 [rad^{-1}]	C_5 [rad^{-1}]	C_6 [rad^{-1}]	thickness [rad]
1	-0.142 ± 0.026	-0.330 ± 0.018	0.080 ± 0.009	0.116 ± 0.158	-0.011 ± 0.040	0.117 ± 0.021	0.022 ± 0.002
2	-0.057 ± 0.018	-0.180 ± 0.047	0.098 ± 0.038	-0.499 ± 0.308	-0.035 ± 0.049	-0.085 ± 0.066	0.022 ± 0.006
3	-0.160 ± 0.041	-0.137 ± 0.050	0.004 ± 0.040	0.112 ± 0.228	-0.006 ± 0.194	0.070 ± 0.076	0.027 ± 0.006
4	-0.174 ± 0.037	-0.304 ± 0.115	0.007 ± 0.023	0.019 ± 0.152	-0.094 ± 0.054	0.069 ± 0.070	0.021 ± 0.009
5	0.020 ± 0.054	-0.205 ± 0.096	0.122 ± 0.046	-0.257 ± 0.360	-0.231 ± 0.100	0.068 ± 0.040	0.024 ± 0.006
6	-0.155 ± 0.038	-0.131 ± 0.106	0.099 ± 0.033	-0.159 ± 0.172	-0.142 ± 0.069	0.247 ± 0.081	0.031 ± 0.009
7	-0.353 ± 0.010	-0.126 ± 0.052	0.074 ± 0.016	-0.060 ± 0.222	0.110 ± 0.070	0.219 ± 0.105	0.024 ± 0.007
8	-0.136 ± 0.022	-0.094 ± 0.080	-0.116 ± 0.040	-0.357 ± 0.373	0.067 ± 0.139	0.135 ± 0.091	0.029 ± 0.012
9	-0.303 ± 0.030	-0.217 ± 0.072	0.135 ± 0.065	-0.147 ± 0.210	-0.243 ± 0.177	0.262 ± 0.137	0.037 ± 0.007
10	-0.185 ± 0.039	-0.131 ± 0.040	0.221 ± 0.038	0.224 ± 0.272	-0.306 ± 0.114	-0.002 ± 0.032	0.023 ± 0.006
overall	-0.164 ± 0.107	-0.186 ± 0.101	0.072 ± 0.094	-0.101 ± 0.319	-0.089 ± 0.168	0.110 ± 0.128	0.026 ± 0.008

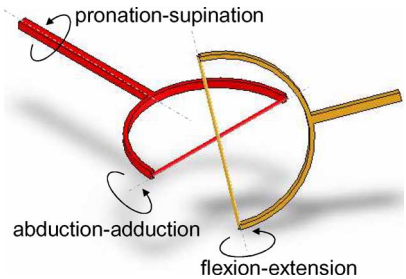

Fig. 5. Sequence of rotations for the mechanism of the wrist robot, derived from [29], used to determine the sequence of matrix multiplication as in (10). Going from distal to proximal: flexion–extension, abduction–adduction, and then, pronation–supination.

can be sensed (and actuated by the robot): 1) $\theta_{\rm PS}$ (pronation–supination); 2) $\theta_{\rm AA}$ (abduction–adduction); and 3) $\theta_{\rm FE}$ (flexion–extension). Knowledge of the sequence, from proximal to distal, of the mechanical joints allows to determine the wrist orientation R_w from the angles as sensed by the wrist module

$$R_w = R_x(\theta_{\rm PS})R_y(\theta_{\rm AA})R_z(\theta_{\rm FE}) \tag{10}$$

where x, y, and z coincide with the axes of the fixed reference frame defined previously (i.e., the primary or "zero" position for the wrist). For a given wrist orientation R_w, the *wrist pointing direction* $\mathbf{n}_w$ is given as in (8).

Once seated, each subject faces a computer screen where a "video game," as shown in Fig. 1, is displayed. The subject is then instructed about the task; starting from the central position, the cursor on the screen shall be moved toward the peripheral positions and, then, back to the central position.

During the execution of each task, data were acquired at a rate of 200 samples/s, in particular, the three sequences of sampled angles $\theta_{{\rm PS}i}, \theta_{{\rm AA}i}$, and $\theta_{{\rm FE}i}$ (where i refers to ith sample at time t_i). Using (10), the sequence of wrist orientation R_{wi} at time t_i was derived. The sequence of wrist pointing directions $\mathbf{n}_i$ was evaluated via (8), and finally, the sequence of rotation vectors $\mathbf{r}_i$ was obtained via (1). The sequence $\mathbf{r}_i = [r_{xi}\ \ r_{yi}\ \ r_{zi}]^T$ was numerically fitted to a generic quadratic surface with coefficients $C_1, \ldots, C_6$ as in (9).

B. Experimental Results for the Wrist Robot

For each subject, the values of the $C_1, \ldots, C_6$ coefficients (as well as of the thickness) averaged over the five trials are reported in each row of Table II and used to define an averaged Donders' surface. Fig. 6(c) shows ten superimposed averaged surfaces: one for each subject. In Fig. 6(d), the averaged coefficients are presented in form of histogram with vertical bars representing the 95% confidence interval.

Remark: The extremely high goodness of fit in terms of thickness (one to two orders of magnitude smaller than in the experiments with the handheld device; compare the rightmost columns of Tables I and II) reveals the absence of any "biological noise" and strongly suggests that the constraint has a mechanical origin rather than a neural one.

Furthermore, with reference to Fig. 6(d), the influence of the mechanism is particularly evident in the Helmholtz-like behavior of the surfaces, in particular, the intersubjectively invariant and positive sign of the C_5 coefficient. It is worth recalling that the Fick and Helmholtz gimbals are 2-D mechanisms, and therefore, their rotation vectors necessarily lie on 2-D surfaces defined in (7), which is a particular case of (9) where all the

TABLE II
EACH ROW REPORTS THE VALUES AVERAGED OVER FIVE TRIALS FOR EACH SUBJECT RELATIVE TO THE TESTS WITH THE WRIST ROBOT

subjects	C_1 [rad]	C_2	C_2	C_4 [rad^{-1}]	C_5 [rad^{-1}]	C_6 [rad^{-1}]	thickness [rad]
1	0.0519 ± 0.0216	-0.0169 ± 0.0379	-0.0110 ± 0.0257	-0.0035 ± 0.0277	0.2339 ± 0.0413	0.0080 ± 0.0038	0.0036 ± 0.0068
2	-0.0485 ± 0.0001	0.0000 ± 0.0008	-0.0015 ± 0.0004	0.0109 ± 0.0037	0.2514 ± 0.0005	-0.0068 ± 0.0010	0.0004 ± 0.0001
3	-0.1376 ± 0.0118	-0.0116 ± 0.0249	0.0009 ± 0.0027	0.0315 ± 0.0726	0.2630 ± 0.0265	-0.0460 ± 0.0370	0.0064 ± 0.0121
4	-0.0368 ± 0.0002	-0.0011 ± 0.0004	-0.0004 ± 0.0003	0.0106 ± 0.0012	0.2536 ± 0.0005	-0.0061 ± 0.0004	0.0002 ± 0.0000
5	-0.0562 ± 0.0002	-0.0004 ± 0.0004	0.0000 ± 0.0002	0.0194 ± 0.0013	0.2519 ± 0.0010	-0.0099 ± 0.0004	0.0002 ± 0.0001
6	-0.0170 ± 0.0109	-0.0006 ± 0.0018	-0.0006 ± 0.0009	0.0025 ± 0.0073	0.2500 ± 0.0026	-0.0027 ± 0.0026	0.0005 ± 0.0002
7	0.1169 ± 0.0131	-0.0058 ± 0.0162	0.0005 ± 0.0032	-0.0764 ± 0.0649	0.2472 ± 0.0051	0.0285 ± 0.0135	0.0022 ± 0.0031
8	-0.0742 ± 0.0002	0.0006 ± 0.0016	-0.0010 ± 0.0005	0.0227 ± 0.0069	0.2519 ± 0.0017	-0.0120 ± 0.0013	0.0004 ± 0.0002
9	-0.1010 ± 0.0262	0.0017 ± 0.0054	0.0043 ± 0.0124	0.1651 ± 0.2926	0.2434 ± 0.0161	-0.0519 ± 0.0745	0.0060 ± 0.0119
10	-0.0340 ± 0.0165	-0.0004 ± 0.0011	-0.0025 ± 0.0025	0.0239 ± 0.0240	0.2537 ± 0.0021	-0.0065 ± 0.0035	0.0017 ± 0.0029
overall	-0.0336 ± 0.0710	-0.0035 ± 0.0151	-0.0011 ± 0.0091	0.0207 ± 0.1054	0.2500 ± 0.0165	-0.0105 ± 0.0330	0.0022 ± 0.0058

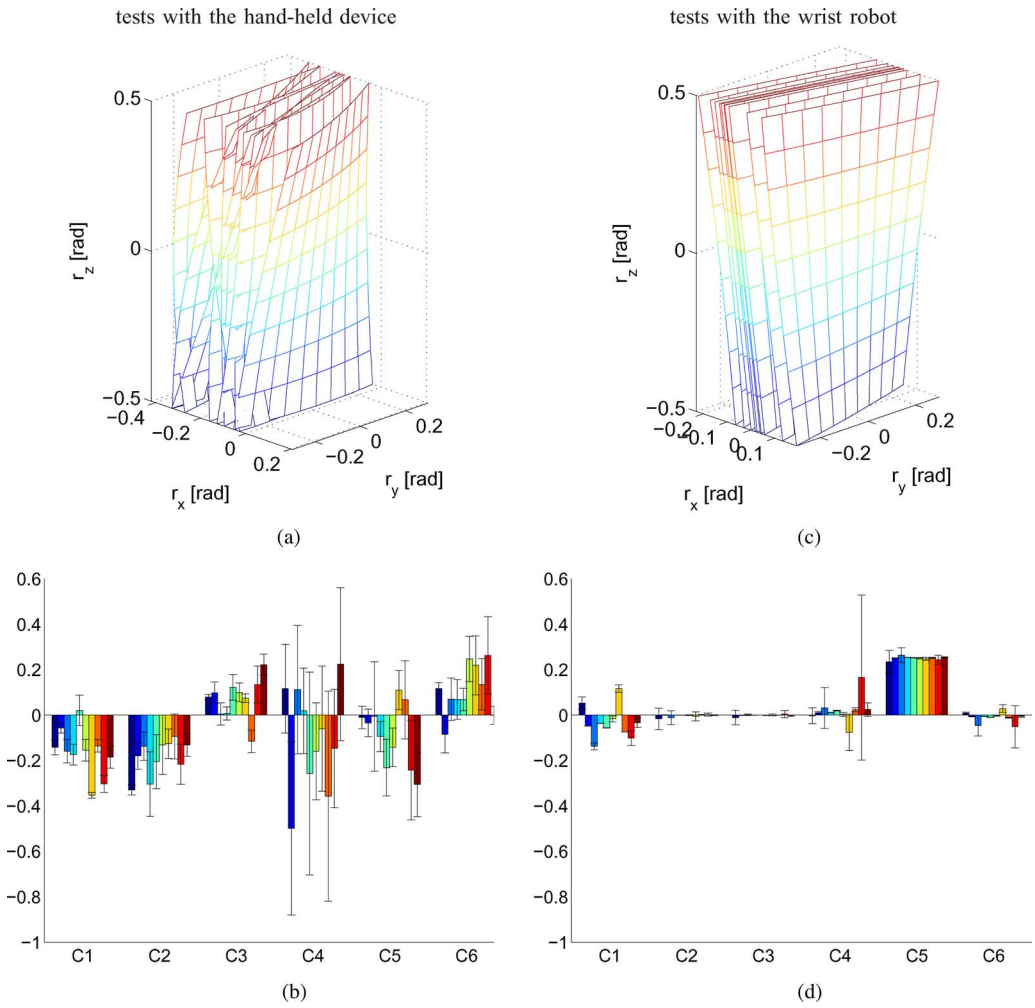

Fig. 6. (a) and (b) Experimental data relative to the tests performed with the handheld device and (c) and (d) with the wrist robot. (Top) Superimposed Donders' surfaces fitting the rotation vectors (in radians) from ten subjects (each surface describes the average outcome from the five trials). (Bottom) Histograms of the $C_1, \ldots, C_6$ coefficients (averaged over five trials, the vertical bars represent the 95% confidence interval) relative to the ten subjects.

coefficients are zero, except for $C_5 = \pm 1/2$. In particular, for the Helmholtz gimbal, $C_5 = 1/2$ holds. A possible explanation for this is that the pronation–supination axis of the robot, i.e., the most proximal axis (see Fig. 5) provides excessive mechanical loading (especially inertial) to the subject, thus limiting the natural torsion of the wrist. When the pronation–supination axis is blocked, the 3-DOF mechanism in Fig. 5 is actually equivalent to the Helmholtz gimbal on the right side of Fig. 2.

C. Comparing Experimental Results

Comparison of the results relative to the handheld devices, with those relative to the wrist robot (see Fig. 6), indicates that the robot mechanisms strongly influence the subjects. In particular, in the experiment with the robot, the fitting surfaces are practically the same from trial to trial and also from subject to subject. Such a statement was demonstrated with a one-way multivariate analysis of variance (MANOVA), where the subjects are the independent variable, and the $C_1, \ldots, C_6$ coefficients are the dependent ones. In the case of the tests with the handheld device, subjects have a statistically significant effect on the six coefficients (their mean values span a full 6-D space). On the contrary, in the case of the wrist robot, the MANOVA test shows that we cannot reject the hypothesis that the mean values of the $C_1, \ldots, C_6$ coefficients lie in a 2-D subspace.

V. Discussion and Conclusion

This paper addresses the issue of back-drivability of rehabilitation robots, during assessment sessions, interacting with a subject involved in redundant motor tasks. In particular, we question whether current design criteria take in due account an important class of constraints that are of neural origin, and therefore intrinsic (or "soft"), and which, different from biomechanical (or "hard") constraints, may or may not arise, depending on the motor task.

This issue has profound clinical implications. In fact, Donders' law (and intrinsic constraints in general) represents a solution implemented by neural mechanisms to motor redundancy and, typically, optimizes motor efficiency. Furthermore, as highlighted by Wong [27] in the domain of eye movements, Donders' law is *plastic* and its adaptability may allow to regain motor efficiency in the case of pathological subjects. Therefore, being able to assess Donders' law is of basic importance as it can provide important indicators for neurorehabilitation. Although the problem is rather general, this paper focuses on the human wrist during pointing tasks. Healthy subjects were asked to perform pointing tasks, while the wrist orientation was assessed by means of a lightweight handheld device to avoid perturbations of any sort. Data from ten subjects show how such intrinsic constraints are well fitted to (2-D) surfaces embedded in the 3-D space of wrist orientations. Such surfaces do not vary much from trial to trial for the same subject but high variability is shown from subject to subject, especially in terms of curvature and twisting of the surface. In particular, this could denote different motor strategies for each subject, i.e., a personal "style" in solving redundancy.

A different group of ten healthy subjects was then asked to complete a similar task while interacting with a state-of-the-art robot for wrist rehabilitation that is designed to fully comply with biomechanical constraints of the human wrist and provide a high degree of back-drivability.

Whereas, in the case of a handheld device, there were statistically significant differences between subjects, in the case of the wrist robot, there was no statistical difference both within subject and between subjects.

Moreover, the very small deviations from the fitting surface, or lack of "biological noise" (as referred to by Tweed and Vilis [26]), denote a mechanical origin of the constraint. This is also compatible with the hypothesis that one of the joints, i.e., the most proximal, may be perceived as too heavy by the subject who resorts to perform the pointing task by deploying the two remaining DOFs. In this sense, the mechanisms of the robot flatten out any personal intrinsic motor strategy or style.

Similar experiments can be generalized and used to test the degree of back-drivability of mechanisms and robots in relation to constraints of neural origin, thus allowing the design of novel robots that can actually cope with such constraints.

As mentioned in this paper, the programmable impedance of the wrist robot was set to zero, i.e., the sole role of the actuators was to compensate gravity, because we were primarily interested in the effect of mechanisms. We expect that the active control of such a robot (e.g., via a sensorized handle) may increase the degree of back-drivability to comply with intrinsic constraints as well. These concepts can be extended to different mechanisms and robots as well, e.g., exoskeletons for the upper or the lower limbs. This will be part of our future work.

Acknowledgment

The authors would like to thank Prof. S. Sterzi and Mr. E. Gallotta, Physical Therapist, for their precious help during the experiments. The authors would also like to acknowledge the feedback and comments of the anonymous reviewers.

References

[1] H. I. Krebs, N. Hogan, M. L. Aisen, and B. T. Volpe, "Robot-aided neurorehabilitation," *IEEE Trans. Rehabil. Eng.*, vol. 6, no. 1, pp. 75–87, Mar. 1998.

[2] H. I. Krebs, M. Ferraro, S. Buerger, M. J. Newbery, A. Makiyama, M. Sandmann, D. Lynch, B. T. Volpe, and N. Hogan, "Rehabilitation robotics: Pilot trial of a spatial extension for MIT-Manus," *IEEE Trans Neural Syst. Rehabil. Eng.*, vol. 15, no. 5, pp. 327–335, Sep. 2007.

[3] H. I. Krebs, B. T. Volpe, D. Williams, J. Celestino, S. K. Charles, D. Lynch, and N. Hogan, "Robot-aided neurorehabilitation: A robot for wrist rehabilitation," *J. Neuroeng. Rehabil.*, vol. 15, no. 3, pp. 327–335, 2007.

[4] C. G. Burgar, P. S. Lum, P. C. Shor, and H. F. M. Van der Loos, "Development of robots for rehabilitation therapy: The Palo development of robots for rehabilitation therapy: The Palo Alto Stanford experience," *J. Rehabil. Res. Dev.*, vol. 37, no. 6, pp. 663–673, 2000.

[5] P. S. Lum, D. J. Reinkensmeyer, R. Mahoney, W. Z. Rymer, and C. G. Burgar, "Robotic devices for movement therapy after stroke: Current status and challenges to clinical acceptance," *Topics Stroke Rehabil.*, vol. 8, no. 4, pp. 40–53, 2002.

[6] D. J. Reinkensmeyer, L. E. Kahn, M. Averbuch, A. McKenna-Cole, B. D. Schmit, and W. Z. Rymer, "Understanding and treating arm movement impairment after chronic brain injury: Progress with the arm guide," *J. Rehabil. Res. Dev.*, vol. 37, no. 6, pp. 653–662, 2000.

[7] L. E. Kahn, M. L. Zygman, W. Z. Rymer, and D. J. Reinkensmeyer, "Robot-assisted reaching exercise promotes arm movement recovery in chronic hemiparetic stroke: A randomized controlled pilot study," *J. Neuroeng. Rehabil.*, vol. 3, no. 12, 2006.
[8] S. Hesse, C. Werner, D. Uhlenbrock, S. V. Frankenberg, A. Bardeleben, and B. Brandl-Hesse, "An electromechanical gait trainer for restoration of gait in hemiparetic stroke patients: Preliminary results," *Neurorehabil. Neural Repair*, vol. 15, no. 1, pp. 39–50, 2001.
[9] M. Pohl, C. Werner, M. Holzgraefe, G. Kroczek, J. Mehrholz, I. Wingendorf, G. Hoölig, R. Koch, and S. Hesse, "Repetitive locomotor training and physiotherapy improve walking and basic activities of daily living after stroke: A single-blind, randomized multicentre trial (Deutsche Gangtrainerstudie, DEGAS)," *Clin. Rehabil.*, vol. 21, no. 1, pp. 17–27, 2007.
[10] G. Colombo, M. Joerg, R. Schreier, and V. Dietz, "Treadmill training treadmill training of paraplegic patients using a robotic orthosis," *J. Rehabil. Res. Dev.*, vol. 37, no. 6, pp. 693–700, 2000.
[11] G. Colombo, R. Riener, and L. Lünenburger, "Human-centered robotics applied to gait training and assessment," *J. Rehabil. Res. Dev.*, vol. 43, no. 5, pp. 679–694, 2006.
[12] D. Reinkensmeyer, N. Hogan, H. I. Krebs, S. L. Lehman, and P. S. Lum, "Rehabilitators, robots and guides: New tools for neurological rehabilitation," in *Biomechanics and Neural Control of Posture and Movement*, J. Winters and P. E. Crago, Eds. New York: Springer-Verlag, 2000, pp. 516–534.
[13] H. I. Krebs, J. J. Palazzolo, L. Dipietro, M. Ferraro, J. Krol, K. Rannekleiv, B. T. Volpe, and N. Hogan, "Rehabilitation robotics: Performance-based progressive robot-assisted therapy," *Auton. Robots*, vol. 15, pp. 7–20, 2003.
[14] D. A. Lawrence, "Impedance control stability properties in common implementations," in *Proc. IEEE Int. Conf. Robot. Autom.*, 1988, pp. 1185–1191.
[15] N. Bernstein, *The Co-ordination and Regulation of Movements*. Oxford, U.K.: Pergamon, 1967.
[16] T. Flash and N. Hogan, "The coordination of arm movements: An experimentally confirmed mathematical model," *J. Neurosci.*, vol. 5, pp. 1688–1703, 1985.
[17] Y. Uno, M. Kawato, and R. Suzuki, "Formation and control of optimal trajectory in human multijoint arm movement," *Biol. Cybern.*, vol. 61, pp. 89–101, 1989.
[18] C. M. Harris and D. M. Wolpert, "Signal-dependent noise determines motor planning," *Nature*, vol. 394, pp. 780–784, 1998.
[19] J. P. Scholz and G. Schoner, "The uncontrolled manifold concept: Identifying control variable for a functional task," *Exp. Brain Res.*, vol. 126, pp. 289–306, 1999.
[20] M. L. Latash, J. P. Scholz, and G. Schoner, "Toward a new theory of motor synergies," *Motor Control*, vol. 11, pp. 276–308, 2007.
[21] M. Fetter, T. Haslwanter, H. Misslich, and D. Tweed, Eds., *Three-Dimensional Kinematics of the Eye, Head and Limb Movements*. Amsterdam, The Netherlands: Harwood, 1997.
[22] P. Viviani and R. Schneider, "A developmental study of the relationship between geometry and kinematics in drawing movements," *J. Exp. Psychol.*, vol. 12, no. 11, pp. 198–218, 1991.
[23] J. F. Soechting and C. A. Terzuolo, "Organization of arm movements in three-dimensional space. Wrist motion is piecewise planar," *J. Neurosci.*, vol. 23, pp. 53–61, 1987.
[24] P. Morasso, "Three dimensional arm trajectories," *Biol. Cybern.*, vol. 48, pp. 187–194, 1983.
[25] F. Lacquaniti, C. A. Terzuolo, and P. Viviani P, "The law relating kinematic and figural aspects of drawing movements," *Acta Psychol.*, vol. 54, pp. 115–130, 1983.
[26] D. Tweed and T. Vilis, "Geometric relations of eye position and velocity vectors during saccades," *Vis. Res.*, vol. 30, no. 1, pp. 111–127, 1990.
[27] A. M. F. Wong, "Listing's law: Clinical significance and implications for neural control," *Surv. Ophthalmol.*, vol. 49, no. 6, pp. 563–575, 2004.
[28] D. G. Liebermann, A. Biess, J. Friedman, C. C. A. M. Gielen, and T. Flash, "Intrinsic joint kinematic planning. I: Reassessing the Listing's law constraint in the control of three- dimensional arm movements," *Exp. Brain Res.*, vol. 171, pp. 139–154, 2006.
[29] D. J. Williams, H. I. Krebs, and N. Hogan, "A robot for wrist rehabilitation," in *Proc. 23rd EMBS Int. Conf.*, Istanbul, Turkey, Oct. 25–28, 2001, pp. 1336–1339.
[30] K. Hepp, "On Listing's law," *Commun. Math Phys.*, vol. 132, pp. 285–292, 1990.
[31] T. Haslwanter, "mathematics of three-dimensional eye rotations," *Vis. Res.*, vol. 35, no. 12, pp. 1727–1739, 1995.
[32] A. A. Handzel and T. Flash, "The geometry of eye rotations and Listing's law," in *Advances in Neural Information Processing Systems 8*, D. Touretzky, M. Mozer, and M. Hasselmo, Eds. Cambridge, MA: MIT Press, 1996, pp. 117–123.
[33] R. M. Murray, Z. Li, and S. S. Sastry, *A Mathematical Introduction to Robotic Manipulation*. Boca Raton, FL: CRC, 1994.
[34] G. Wu, S. Siegler, P. Allard, C. Kirtley, A. Leardini, D. Rosenbaum, M. Whittle, D. D. D'Lima, L. Cristofolini, H. Witte, O. Schmid, and I. Stokes, "ISB recommendation on definitions of joint coordinate systems of various joints for the reporting of human joint motion—Part II: Shoulder, elbow, wrist and hand," *J. Biomech.*, vol. 38, pp. 981–992, 2005.
[35] M. P. Do Carmo, *Differential Geometry of Curves and Surfaces*. Englewood Cliffs, NJ: Prentice–Hall, 1976.

Domenico Campolo (M'09) received the Laurea degree from the University of Pisa, Pisa, Italy, in 1998, the Diploma in engineering from the Scuola Superiore Sant'Anna, Pisa, in 1999, and the Ph.D. degree in microengineering from the MiTech Laboratory (currently the Center of Research in Microengineering Laboratory), Scuola Superiore Sant'Anna, Pisa, in 2002.

During the fall of 1998, he was a Visiting Graduate Student with the Department of Electrical Engineering and Computer Science, ZheJiang University, HangZhou, China. During 2000–2003, he was a Visiting Scholar with the University of California, Berkeley, where he was a Postdoctoral Fellow for the Micromechanical Flying Insect Project after 2002. Since October 2003, he has been with the Università Campus Bio-Medico, Rome, Italy, where he is involved in both teaching and research and is currently an Assistant Professor. In particular, he is a Project Manager of the Thought in ACTion (TACT) Project, funded by the European Union under the New and Emerging Science and Technology Program. His current research interests include mechatronic technologies with application to the new emerging fields of phenomics and neurodevelopmental engineering in both animal and human models and biomimetic microrobotics, including design, fabrication, development, and control of biologically inspired smart actuators and sensors. He is the author or coauthor of more than 35 peer-reviewed papers in international journals and conference proceedings.

Dino Accoto (M'06) received the Laurea degree (*cum laude*) in mechanical engineering from the University of Pisa, Pisa, Italy, in 1998 and the Diploma (*cum laude*) in engineering and the Ph.D. degree (*cum laude*) in biomedical robotics from the Scuola Sant'Anna, Pisa, in 1999 and 2002, respectively.

From October 2001 to September 2002, he was a Visiting Researcher with the Rapid Prototyping Laboratory, Stanford University, CA. From 2003 to 2007, he was an Assistant Professor of biomedical engineering at the Scuola Sant'Anna. Since 2004, he has been with the Biomedical Robotics and Biomicroengineering Laboratory, Università Campus Bio-Medico, Rome, Italy, where he is currently an Assistant Professor of biomedical engineering. His current research interests include the development of novel mechatronic systems for biomedicine and biorobotics, possibly taking advantage of a purposively designed physical interaction between the artifact and the human body. He has authored or coauthored more than 50 papers appearing in international journals and conference proceedings and holds six patents.

Domenico Formica was born in Italy in 1980. He received the B.S. and M.S. degrees in biomedical engineering and the Ph.D. degree in bioengineering from the Università Campus Bio-Medico, Rome, Italy, in 2002, 2004, and 2008, respectively.

From May to November 2007, he was a Visiting Student at the Newman Laboratory for Biomechanics and Human Rehabilitation, Massachusetts Institute of Technology, Cambridge, where he was involved in the field of new robot-based algorithms for quantitative measure of muscular tone in patients with neurological injuries, with particular attention to the estimation of the passive stiffness of the wrist joint. Since May 2008, he has been a Postdoctoral Fellow with the Laboratory of Biomedical Robotics and Biomicrosystems, Università Campus Bio-Medico, where he is involved in the development and experimental design of mechatronic systems for monitoring the behavior of children and their application to early diagnosis of neurodevelopmental disorders. His current research interests include the areas of mechatronic technologies for the study of human motor control, with particular attention to neurodevelopment, quantitative algorithms for clinical assessment of patients with neuromuscular disorders, and novel robotic devices for rehabilitation motor therapy after neurological injury, with special attention to the issue of interaction control.

Eugenio Guglielmelli (S'92–M'95) received the Laurea degree in electronics engineering and the Ph.D. degree in electronics, computer science, and telecommunications (biomedical robotics track) from the University of Pisa, Pisa, Italy, in 1991 and 1995, respectively.

He is currently an Associate Professor of bioengineering with the Università Campus Bio-Medico, Rome, Italy, where he is also the Head of the Laboratory of Biomedical Robotics and Biomicrosystems. From 1991 to 2004, he was with the Scuola Superiore Sant'Anna, Pisa, where he was the Coordinator of the Advanced Robotics Technology and Systems Laboratory during 2002–2004. His current research interests include the fields of human-centered robotics, biomechatronic design and biomorphic control of robotic systems, and their application to rehabilitation, personal assistance, and neurorobotics. He is a Principal Investigator/Partner of several national and international projects in the area of biomedical robotics. He is author or coauthor of more than 150 papers appearing in peer-reviewed international journals, conference proceedings, and books. He is a coinventor of three patents. He is a member of the Editorial Board of the *International Journal on Applied Bionics and Biomechanics*. He was a Guest Co-Editor of the Special Issue on Rehabilitation Robotics of the International Journal *Autonomous Robots* and a Guest Co-Editor of the Special Issue on Robotics Platforms for Research in Neuroscience of the Robotics Society of Japan International Journal *Advanced Robotics*. In 1998, he was a Visiting Researcher at Waseda University, Tokyo, Japan.

Dr. Guglielmelli is currently serving as an Associate Editor of the *IEEE Robotics and Automation Magazine*. He is a member of the IEEE Robotics and Automation Society (RAS), the IEEE Engineering in Medicine and Biology Society, and the Society for Neuroscience. He is currently the Associate Vice President for Technical Activities of the IEEE RAS, where he was a Secretary (2002–2003) and a Co-Chair of the Technical Committee on Rehabilitation and Assistive Robotics (2004–2007). He was the General Co-Chair of the 1999 International Conference on Humanoid Robotics (Tokyo, Japan) and Chair of the 5th International Advanced Robotics Programme/IEEE RAS/European Robotics Research Network Workshop on *Technical Challenges for Dependable Robots in Human Environments* (Rome, Italy, 2007). He has been a member of the organizing and/or program committees of many other international conferences, and workshops, mainly sponsored by IEEE RAS.